Dust Grains Cannot Grow to Millimeter Sizes in Protostellar Envelopes

Kedron Silsbee[1,2] , Vitaly Akimkin[3] , Alexei V. Ivlev[1] , Leonardo Testi[4,5] , Munan Gong[1] , and Paola Caselli[1]

[1] Max-Planck-Institut für Extraterrestrische Physik, 85748 Garching, Germany; ksilsbee@mpe.mpg.de
[2] University of Texas at El Paso, El Paso, TX, 79968, USA
[3] Institute of Astronomy, Russian Academy of Sciences, 48 Pyatnitskaya St., Moscow 119017, Russia
[4] European Southern Observatory, Karl-Schwarzschild-Str. 2, D-85748 Garching bei München, Germany
[5] INAF-Osservatorio Astrofisico di Arcetri, Largo E. Fermi 5, I-50125 Firenze, Italy

Abstract

A big question in the field of star and planet formation is the time at which substantial dust grain growth occurs. The observed properties of dust emission across different wavelength ranges have been used as an indication that millimeter-sized grains are already present in the envelopes of young protostars. However, this interpretation is in tension with results from coagulation simulations, which are not able to produce such large grains in these conditions. In this work, we show analytically that the production of millimeter-sized grains in protostellar envelopes is impossible under the standard assumptions about the coagulation process. We discuss several possibilities that may serve to explain the observed dust emission in the absence of in situ grain growth to millimeter sizes.

Unified Astronomy Thesaurus concepts: Dust physics (2229); Star forming regions (1565); Planet formation (1241)

1. Introduction

One of the key steps in the formation of planets is the growth of dust particles from the submicron-sized grains in the interstellar medium to pebble-sized aggregates. It is generally thought that this growth occurs in protoplanetary disks, which indeed show widespread evidence for the presence of large grains (e.g., Testi et al. 2014). Nevertheless, evidence has accumulated in the last decade, suggesting that dust evolution begins already in clouds and cores (before the formation of protoplanetary disks), where infrared observations have convincingly shown the presence of a significant population of grains grown to a few microns (Pagani et al. 2010). More recent millimeter observations of the spectral index of dust emission appear to be consistent with the presence of millimeter-sized grains in the inner region of class 0 protostellar envelopes (e.g., Kwon et al. 2009; Miotello et al. 2014; Galametz et al. 2019). These latter results are surprising, because taken at face value, they appear to be at odds with the expected timescales for grain growth in cores and envelopes of protostars. Simulations of grain coagulation typically do not predict growth beyond tens of microns (e.g., Ossenkopf 1993; Ormel et al. 2009) Li et al. (2017), Galametz et al. (2019), and Agurto-Gangas et al. (2019) have shown that the derivation of the grain growth constraints from the spectral index is not always straightforward, and that not all protostars show definitive evidence for grain growth. Nonetheless, through a careful analysis of a large sample of protostellar envelopes, Galametz et al. (2019) show evidence of the possible presence of millimeter-size grains in the inner ∼500 au of at least some protostellar envelopes. Indirect evidence from mm polarization observations seems to confirm the inferred presence of grains of at least 10 μm (see, e.g., Valdivia et al. 2019). It is thus important to revisit the modeling of grain growth in cores and

protostars, with the aim of understanding whether growth to millimeter sizes in these environments is indeed possible under certain circumstances.

There have been many studies of dust coagulation in molecular clouds and prestellar cores. Rossi et al. (1991) considered the growth of dust grains via coagulation and condensation of gas-phase molecules in a cloud undergoing pressure-free spherical collapse. They assumed the grain velocities to arise in response to gas turbulence. Because of the rapid collapse in their model and the fact that the possibility of fractal growth/high grain porosity was not considered, they were only able to grow grains of a few microns in size. A wider range of possible sources of collision velocity (turbulence, Brownian motion, and motions arising from grain asymmetries and differential gravitational settling) was considered by Ossenkopf (1993). He found the dominant driver of coagulation to be turbulence at number densities below $10^8 \, \mathrm{cm}^{-3}$, and Brownian motion at higher densities. He did not run the simulations for long enough to see the growth of large grains. Ormel et al. (2009) considered collision velocities arising in response to turbulence in the gas, and developed a detailed model for collision outcomes including sticking, fragmentation and compaction. They considered evolution timescales as long as 10^7 yr at densities of $10^7 \, \mathrm{cm}^{-3}$ and were able to grow grains up to 0.6 mm in size, with the maximum size determined by fragmentation. Recently, Silsbee et al. (2020) and Guillet et al. (2020) considered an additional mechanism leading to relative velocity—the differential coupling of grains of different sizes to the neutral and magnetized component of the gas. They both found that it resulted in a very rapid removal of the smallest grains from the size distribution, but had little effect on the maximum grain size.

However, there are several uncertain parameters in grain growth models related to the dust physics. Their variation has not been systematically explored in the dust coagulation simulations, partly due to the difficulty of covering a large parameter space. For example, the evolution of the dust porosity is a matter of substantial debate in the literature (e.g., Shen et al. 2008; Wada et al. 2008; Okuzumi et al. 2009;

Ormel et al. 2009), with uncertainty as to whether the grains remain compact or undergo fractal growth. There is also a significant uncertainty in the critical collision velocity required for grain fragmentation, with different theoretical and experimental work pointing to different threshold velocities, from centimeters per second to several tens of meters per second, depending on grain composition and size (Blum & Wurm 2008; Ormel et al. 2009; Wada et al. 2013; Gundlach & Blum 2015; Kimura et al. 2015; Musiolik et al. 2016). Moreover, while much work has assumed a Kolmogorov slope of the turbulent energy spectrum, this need not necessarily be the case. In protoplanetary disks, turbulence driven by the magnetorotational instability was shown to have a shallower power spectrum (Gong et al. 2020). Furthermore, the rate of dust growth was shown to be very sensitive to the slope of the turbulent power spectrum (Gong et al. 2021).

In this paper, we consider a simple but general coagulation model that can be solved analytically. By using the analytic solution, we are able to put rigorous upper bounds on the growth that may take place, without having to numerically explore the many-dimensional space of parameters that affect the coagulation rate. We consider the degree of compaction, the maximum collision velocity that can be sustained without fragmentation, and the normalization and slope of the turbulent power spectrum as free parameters.

2. Calculation of the Minimum Grain Growth Timescale

While there is some nontrivial dependence of the optical properties on grain porosity, it is reasonable to approximate that the optical properties of a grain are a function of the product of its size and filling factor (Kataoka et al. 2014, see their Figure 11), i.e.,

$$a_{\mathrm{opt}} = \phi a, \qquad (1)$$

where $\phi < 1$ is the fraction of the grain volume occupied by solid material and a is the grain radius. For grain growth to greatly affect the spectral index at wavelength λ, the grains should have $|m - 1|a_{\mathrm{opt}} \gtrsim \lambda/(2\pi)$, where m is the complex refractive index.

Let us define τ_{coll} as the expected time for a grain to double its mass. We note from the simulations performed in (Silsbee et al. 2020, see top panels of their Figure 7), that, at least for the Kolmogorov turbulence spectrum and compact grains, the grain size distribution remains relatively narrow, even as growth proceeds. We therefore approximate that, at any given time, the size distribution is monodisperse (see Appendix A in Ormel et al. 2009). We verify in the Appendix of this work that this approximation introduces very little error when compared with simulations of the full size distribution. Therefore, τ_{coll} is exactly equal to the expected time for an individual grain to experience a collision:

$$\tau_{\mathrm{coll}} = \frac{1}{n_d \sigma v_{\mathrm{coll}}}, \qquad (2)$$

where σ is the collision cross section, v_{coll} the collision velocity, and the number density n_d can be easily related to the molecular hydrogen number density n_g, the grain size a, dust-to-gas ratio f_d, and size-dependent dust density $\rho_d(a)$:

$$n_d = \frac{3 f_d \rho_g}{4\pi a^3 \rho_d(a)}, \qquad (3)$$

where $\rho_g = n_g \mu_g$ and μ_g is the mean mass per hydrogen molecule. We assumed a gas with five parts molecular hydrogen to one part helium, so $\mu_g = 2.8 m_{\mathrm{H}}$, with m_{H} being the mass of a hydrogen atom. Throughout this work, we assume spherical grains. Also, we assume a geometric cross section $\sigma = 4\pi a^2$, as Coulomb focusing has been shown to be unimportant except for small grains with very small encounter velocities (Akimkin et al. 2020).

As the grains grow, they may not necessarily remain compact. We parameterize this by a fractal dimension $D > 2$, such that the grain density satisfies

$$\rho_d(a) = \rho_s \left(\frac{a}{a_0}\right)^{D-3}, \qquad (4)$$

where $D = 3$ corresponds to compact grains with constant solid density ρ_s, and $D \to 2$ to fractal grains with constant mass to surface area ratio. a_0 is the initial grain size. Noting that the filling factor $\phi = \rho_d/\rho_s$, Equations (1) and (4) imply the following relation between size a and the optical equivalent size:

$$\left(\frac{a}{a_0}\right)^{D-2} = \frac{a_{\mathrm{opt}}}{a_0}. \qquad (5)$$

We consider collision velocities arising in response to turbulence in the gas, as these are thought to dominate for grains larger than $0.1\ \mu$m (Silsbee et al. 2020). This turbulence need not necessarily have a Kolmogorov power spectrum. We let p be the slope of the power spectrum of the turbulence ($5/3$ for Kolmogorov turbulence). Gong et al. (2021) showed (see Equation (30) therein; note that for equal particle sizes, the prefactor of the nonvanishing term in that equation should include an additional factor of 2) that, if both grains have Stokes number St $\ll 1$, and the eddy correlation time is equal to the eddy turnover time, we can write the collision velocity between two grains of equal sizes as

$$v_{\mathrm{coll}} = v_g \psi(p) \mathrm{St}^q, \qquad (6)$$

where v_g is the turbulent velocity, $\psi(p) = \sqrt{8(p-1)/(p+1)}$ is a factor of order unity, and $q = (p-1)/(3-p)$; for all turbulence models with $1 < p < 2$, we have $0 < q < 1$. The Stokes number St $= \tau_s/\tau_L$, where $\tau_L = r/(v_g \sqrt{p-1})$ is the eddy turnover time at the injection scale r, and $\tau_s(a) = a\rho_d(a)/(\rho_g v_{\mathrm{th}})$ is the grain stopping time due to gas friction in the Epstein regime (Epstein 1924). Here, $v_{\mathrm{th}} = 0.92\sqrt{4k_B T/\pi m_{\mathrm{H}}}$ is the mean thermal velocity of the H$_2$ particles, with a correction factor of 0.92 to account for the presence of helium.

Combining Equations (2) through (6), we find

$$\tau_{\mathrm{coll}}(a) = \frac{a\rho_d(a)}{3 f_d n_g \mu_g v_g \psi(p)} \left(\frac{n_g \mu_g v_{\mathrm{th}} r}{a \rho_d(a) v_g \sqrt{p-1}}\right)^q. \qquad (7)$$

To solve for the time evolution of the size distribution, we note that $\dot{a}/a = \frac{1}{D}\dot{m}/m$. We can then write

$$\frac{da}{dt} = \frac{a}{D\tau_{\mathrm{coll}}(a)}. \qquad (8)$$

Table 1
Fiducial Parameters

Symbol	Meaning	Fiducial Value
r	length scale of environment	1000 au
τ_{env}	lifetime of Class 0 stage	10^5 yr
p	slope of turbulent energy spectrum	5/3
q	$(p-1)/(3-p)$	1/2
T	temperature	20 K
μ_g	mean mass per hydrogen molecule	$2.8 m_{\mathrm{H}}$
n_g	number density of hydrogen molecules	10^7 cm^{-3}
ρ_s	dust material density	3 g cm^{-3}
f_d	dust-to-gas mass ratio	0.01
a_0	initial grain size	1 μm
D	fractal dimension of grain growth	3
v_{max}	grain fragmentation velocity	10 m s^{-1}

Substituting Equation (7) for τ_{coll}, we obtain the solution

$$a(t) = a_0 \left[\frac{(1-q)(D-2)t}{D\tau_{\mathrm{coll}}(a_0)} + 1 \right]^{\frac{1}{(1-q)(D-2)}}. \quad (9)$$

Using Equation (9), we can solve for the growth time τ_{gr} at which the grain reaches size a:

$$\tau_{\mathrm{gr}} = \frac{D\tau_{\mathrm{coll}}(a_0)}{(1-q)(D-2)} \left[\left(\frac{a}{a_0} \right)^{(1-q)(D-2)} - 1 \right] \leqslant \tau_{\mathrm{env}}, \quad (10)$$

where τ_{env} is the lifetime of the envelope. Note that, for $D \to 2$, the grain growth becomes exponential, $a(t) = a_0 e^{t/2\tau_{\mathrm{coll}}(a_0)}$, and then the condition in Equation (10) is reduced to $2\tau_{\mathrm{coll}}(a_0)\ln(a/a_0) \leqslant \tau_{\mathrm{env}}$.

If the collision velocities are too high, then the grains may shatter instead of sticking when they collide. We parameterize this by assuming that there is a (size-independent) maximum collision velocity v_{max} above which grain fragmentation occurs. The highest-speed collisions will be between the largest grains. Because of this, and the fact that the threshold velocity for sticking is generally thought to decrease with size (see, e.g., Wada et al. 2013), v_{max} may be thought of as the threshold velocity for the largest grains. Requiring the collision velocity between two grains of size a to be less than v_{max} gives the relation

$$v_g \psi(p) \left(\frac{a_{\mathrm{opt}} \rho_s v_g \sqrt{p-1}}{n_g \mu_g v_{\mathrm{th}} r} \right)^q \leqslant v_{\mathrm{max}}. \quad (11)$$

2.1. Fiducial Parameters

In what follows, we keep our derivations fully general, but we do provide a few numerical estimates and a figure. These are made for the specific parameters listed in Table 1.

2.2. Results

Based on the observations of low spectral index of the dust emission between 1.3 and 3.2 mm shown in Galametz et al. (2019), we are interested in growing grains that have a_{opt} around 1 mm. Equations (10) and (11) define two regions in the plane of v_g and n_g, which are "acceptable" in the sense of having sufficiently rapid coagulation without introducing excessive collisional velocities. Equations (10) and (11) can
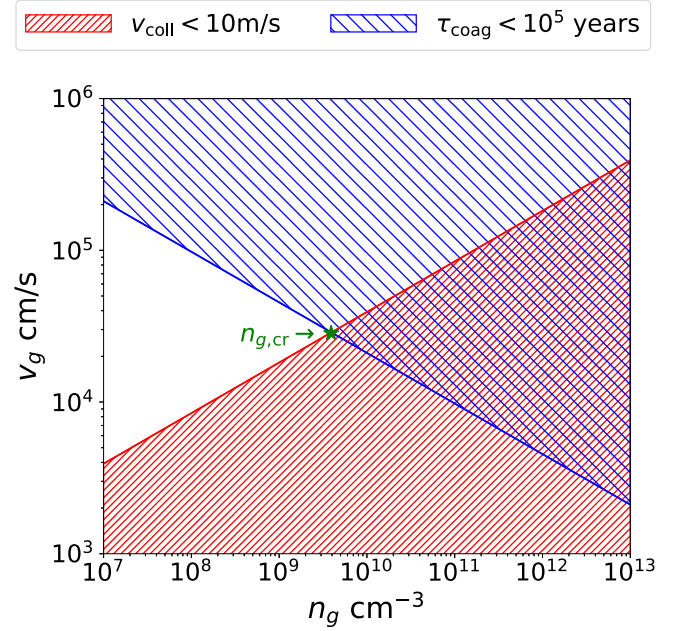
Figure 1. Regions of n_g–v_g space in which the maximum collision velocity is below v_{max} (red shading; see Equation (11)), and the timescale for grain growth to 1 mm is below τ_{env} (blue shading; see Equation (10)). This is made assuming the fiducial parameters in Table 1. The region with overlapping red and blue shading is the allowed parameter space for grain growth to 1 mm. The star corresponds to the critical density above which this is possible (see Equation (15)).

be written in the form

$$\mathscr{G} v_g^{-1-q} n_g^{q-1} \leqslant 1, \qquad \mathscr{F} v_g^{1+q} n_g^{-q} \leqslant 1, \quad (12)$$

where

$$\mathscr{G} = \frac{a_0 \rho_s D}{3\mu_g f_d \tau_{\mathrm{env}} \psi(p)(1-q)(D-2)} \left(\frac{\mu_g v_{\mathrm{th}} r}{a_0 \rho_s \sqrt{p-1}} \right)^q$$

$$\times \left[\left(\frac{a_{\mathrm{opt}}}{a_0} \right)^{1-q} - 1 \right], \quad (13)$$

and

$$\mathscr{F} = \frac{\psi(p)}{v_{\mathrm{max}}} \left(\frac{a_0 \rho_s \sqrt{p-1}}{\mu_g v_{\mathrm{th}} r} \right)^q \left(\frac{a_{\mathrm{opt}}}{a_0} \right)^q. \quad (14)$$

Equations (12) are plotted in Figure 1. The requirement that $v_{\mathrm{coll}} \leqslant v_{\mathrm{max}}$ provides an upper bound on v_g, and the requirement that $\tau_{\mathrm{gr}} \leqslant \tau_{\mathrm{env}}$ provides a lower bound on v_g. At low density, we cannot simultaneously satisfy these requirements, but above some density, the regions overlap. For our fiducial parameters, Figure 1 shows that this critical density is about 4×10^9 cm^{-3}. We note that the corresponding value of the turbulent velocity v_g is a very reasonable 3×10^4 cm s^{-1}, which corresponds to an isothermal Mach number of 1.1

The doubly shaded region that satisfies both Equations (10) and (11) exists to the right of the intersection point of the two curves. Replacing the "$\leqslant$" signs in Equation (12) with "$=$" and multiplying the two equations together yields the critical value

$n_{g,cr} = \mathscr{F}\mathscr{G}$ of gas density at the intersection point:

$$n_{g,cr} = \frac{a_0 \rho_s D}{3 \mu_g f_d \tau_{env}(1 - q)(D - 2)v_{max}} \left[\frac{a_{opt}}{a_0} - \left(\frac{a_{opt}}{a_0} \right)^q \right]$$

$$= 3.9 \times 10^9 \left(\frac{a_{opt}}{1 \text{ mm}} \right) \left(\frac{10^5 \text{ yr}}{\tau_{env}} \right) \left(\frac{10 \text{ m s}^{-1}}{v_{max}} \right) \text{ cm}^{-3},$$

$$(15)$$

where in the numerical estimate we ignore the small second term in the square brackets and take the fiducial parameters from Table 1. Remarkably, the slope p of the turbulent power spectrum has little effect on the critical value of n_g. This is because of the condition that the collision speed of the largest bodies be no more than v_{max}. For all the values of p that we consider, the growth timescale $\tau_{coll}(a)$ increases with a (see Equation (7)). For this reason, the total growth timescale is dominated by the time taken by the final few doublings in size. The collision velocity for these sizes will be on the order of v_{max}, no matter what value of p we take (because we are bound by the condition that $v_{coll} = v_{max}$ at the maximum size). A shallower spectrum means that this maximum size is achievable with a lower value of v_g, but because we assume no prior knowledge of v_g, this does not affect our result. For our fiducial parameters, and a_{opt} deduced from the numerical estimate in Equation (15), with $n_{g,cr} = n_g$ the implied value of v_g is 210 m s^{-1}. For steeper spectra of the turbulence (larger values of p), the required values of v_g may become unrealistically large. This simply means that, in this case, the grain growth will proceed even more slowly than our calculations would suggest.

Furthermore, the critical density is insensitive to changes in the fractal dimension D, unless D becomes close to 2, in which case $n_{g,cr}$ diverges. One can also think of a situation where $D = 3$, but the filling factor ϕ is much less than unity. In this case, $\rho_d/\rho_s = a_{opt}/a = \phi$, and we readily derive the expression for $n_{g,cr}$, which coincides with Equation (15) for $D = 3$ (again, ignoring the second term in the square brackets).

2.3. Maximum Grain Size

Assuming $a_{opt} \gg a_0$, we can drop the second term in parentheses in Equation (15) and solve for a_{opt}, leaving us with

$$a_{opt} = \frac{3 \mu_g f_d (1 - q)(D - 2)}{\rho_s D} n_g \tau_{env} v_{max}$$

$$= 2.5 \left(\frac{n_g}{10^7 \text{ cm}^{-3}} \right) \left(\frac{\tau_{env}}{10^5 \text{ yr}} \right) \left(\frac{v_{max}}{10 \text{ m s}^{-1}} \right) \mu\text{m}. \quad (16)$$

The numerical estimate assumes the fiducial value of all well-constrained parameters that are not explicitly listed. Because v_g could be smaller than the maximum value permitted by the condition $v_{coll} \leqslant v_{max}$, Equation (16) is an upper bound on the possible grain growth.

Based on a study of relative abundances of different stages of protostars, Evans et al. (2009) estimated a mean lifetime for class 0 protostars of $\tau_{env} = 1.0 \times 10^5$ yr. We note that this provides an upper limit on the time available for coagulation in this phase. The existence of an envelope for 10^5 yr does not necessarily imply that the *same* material is present in the

envelope for the whole time. Due to infall motion, it may be that the material currently present in the observed envelopes has been at that density for much less than 10^5 yr, and would thus display even less dust growth. On the other hand, one could imagine that some growth has taken place in the prestellar phase, but this effect is unlikely to be significant (see Section 3.1.2).

Kristensen et al. (2012) modeled the dust emission in a sample of 15 class 0 sources. Based on their modeling, at a distance of 500 au from the central star, the mean density is $n_g = 7 \times 10^6 \text{ cm}^{-3}$ with a range from $1 \times 10^6 \text{ cm}^{-3}$ to $2 \times 10^7 \text{ cm}^{-3}$. Following Birnstiel et al. (2012), we take $v_{max} = 10 \text{ m s}^{-1}$.

Using the fiducial parameters given in Section 2.1, we find $a_{opt} = 2.5 \text{ } \mu\text{m}$. One could imagine a factor of a few change in f_d/ρ_s coming from the effect of freeze-out (see Section 3.1.1), but even taking this into account, we would have to increase the product $n_g \tau_{env} v_{max}$ by two orders of magnitude to account for mm-sized grains in these cores.

Equation (6) is derived assuming that the Stokes numbers remain small. For $10^5 \text{ cm}^{-3} \leqslant n_g \leqslant 10^9 \text{ cm}^{-3}$, $10^4 \text{ yr} \leqslant \tau_{env} \leqslant 10^6 \text{ yr}$, $2.1 \leqslant D \leqslant 3.0$, and $1.05 \leqslant p \leqslant 1.95$ (and other parameters taken from Table 1), we calculated the maximum grain size using Equation (16) and then calculated the Stokes number for grains of that size. For all cases in which the first term in brackets in Equation (15) is more than twice the second (so that dropping the second in favor of the first, as we do in Equation (16), is reasonable), we find that the Stokes number for grains of size a_{opt} is less than 5×10^{-3}, thus justifying this approximation.

It is somewhat counterintuitive that the maximum grain size (Equation (16)) is almost independent of q (or equivalently p, the slope of the turbulent energy spectrum). In contrast, it was found in Gong et al. (2021) that the coagulation rate is highly sensitive to this parameter. This apparent discrepancy arises due to different assumptions about what is held fixed as p varies. In Gong et al. (2021), the value of α, which determines the turbulent velocity is a fixed quantity. In their work, the turbulent velocity is assumed to be low enough that fragmentation can be ignored. In contrast, in the present work, because we are trying to derive an upper bound on the dust size, we are implicitly varying v_g as we vary p, so that Equation (11) remains satisfied.

3. Discussion

In this section, we explore some of the uncertainties in our model, and discuss the plausibility of some alternate hypotheses not involving large dust grains, to explain the observed low spectral indices.

3.1. Model Uncertainties

Here, we analyze the possible impact of some poorly constrained processes neglected in the above consideration.

3.1.1. Possible Effects of Freeze-out

The observations motivating this paper correspond to distances from the central star of a few hundred to few thousand au (Kwon et al. 2009; Miotello et al. 2014; Galametz et al. 2019). The temperature at these distances varies significantly, depending on the assumed stellar luminosity and dust distribution. Galametz et al. (2019) find temperatures

ranging from 28 to 62 K at 200 au and from 11 to 25 K at 2000 au. At these temperatures, we expect that at least some of the volatile material will be frozen-out on the surface of the dust grains. This means that the typically used dust density of 3 g cm^{-3} and dust-to-gas ratio 0.01 may no longer be appropriate to use. The total mass of dust can be obtained by adding up the contribution from all metals excepting the noble gases. Using a solar metallicity, this gives a maximum dust-to-gas ratio of 1.2% (Asplund et al. 2009). This practically coincides with our fiducial value of 1.0%. The additional material likely has a density on the order of 1 g cm^{-3}. It therefore seems that the presence of icy mantles will only affect the combination f_d/ρ_s that enters in the maximum value of a_{opt} in Equation (16) by a factor of $\sim$3 at most.

The degree of freeze-out may also have a substantial effect on v_{max}. There is a wide variety of estimates in the literature for the critical fragmentation velocity, depending on grain composition and size. It is generally thought, based on both experimental (e.g., Gundlach & Blum 2015) and theoretical studies (e.g., Wada et al. 2008), that the presence of icy mantles increases the stickiness of grains (but see Kimura et al. 2020). However, we have already used a somewhat generous value of $v_{max} = 10$ m s^{-1}, as adopted in Birnstiel et al. (2012), justified there as appropriate for ice-coated grains.

In addition to any effect on the coagulation process, icy mantles covering refractory grains in dense and cold regions may dramatically change the dust opacity. The commonly used opacity model of Ossenkopf & Henning (1994) predicts a broad absorption feature in the far-IR range, associated with lattice vibrations of the water ice and leading to significant opacity variations at wavelengths of up to $\approx$200 μm. The form of the opacity function generally depends on the actual ice composition. While there are very few direct measurements of the optical constants of astrophysical ice analogs in the (sub) mm range (see Allodi et al. 2014; Giuliano et al. 2019), these studies indicate the presence of localized, strong absorption features at such wavelengths, and hence suggest possible opacity bumps. Additional measurements of the optical constants in this spectral range are needed to quantify the importance of absorption features and their potential contribution into the opacity index.

3.1.2. Coagulation Prior to the Class 0 Phase

While the present work considers coagulation that occurs during the Class 0 phase, it is possible that some growth begins even prior to this stage. Dust growth in a collapsing cloud was discussed first in Hirashita & Omukai (2009). They used a freefall model for the collapse, and studied the growth assuming the grain velocities to be determined from Brownian motion. Because Brownian motion is only efficient for the smallest grains, they found that grains remained smaller than a micron, even at densities as high as 10^{13} cm^{-3}.

Guillet et al. (2020) treated the collapse using a method similar to that of Hirashita & Omukai (2009), but also included the effects of ambipolar diffusion and turbulence on the collision velocities. The addition of these other sources of motion (turbulence in particular) allowed the formation of $\sim$10 μm grains at the time when the density reached $n_g = 10^{12}$ cm^{-3}. But based on this result, it seems that formation of large grains during the prestellar phase is impossible except in the very dense material (which presumably becomes part of the star, rather than the envelope).

Silsbee et al. (2020) analyzed dust growth in the prestellar stage at a density of $n_g = 7 \times 10^5$ cm^{-3}, assuming a cloud lifetime set by ambipolar diffusion (calculated to be 10 times the freefall time at that density). Even in their most optimistic model, the grain sizes were capped at 10 microns.

Bate (2022) considered the same problem of grain growth in a collapsing prestellar core. He considered relative velocities arising from Brownian motion, pressure gradients, and turbulence. In contrast to Hirashita & Omukai (2009) and Guillet et al. (2020), the grain coagulation was coupled to a 3D SPH simulation of the gas dynamics. Even with this added degree of realism, grain growth at moderate densities was minimal, with the grain size not reaching 10 μm below a number density of 10^{14}–10^{15} cm^{-3}. The lifetime of prestellar cores at a particular density has been shown observationally to be a few times the freefall time at that density, i.e., proportional to $n_g^{-1/2}$ (Könyves et al. 2015). Given that, all else being equal, the maximum coagulation rate is proportional to n_g, the amount of grain growth per logarithmic interval in density is dominated by the highest densities. From these considerations, and the fact that the formation of mm-sized grains is relatively insensitive to the initial size, we consider it unlikely that grain growth in the prestellar phase would significantly alter our conclusions, unless there are mechanisms—such as protostellar outflows (Wong et al. 2016; Tsukamoto et al. 2021)—that eject grains in large amounts from the very dense central region.

3.2. Alternative Explanations for the Observations

In this section, we discuss the plausibility of several different mechanisms that could produce the observed spectral indices without requiring the presence of mm-sized grains

3.2.1. Effects of Temperature and Optical Depth

The presence of large dust grains is inferred from measurements of the spectral index α of dust emission. For two frequencies ν_1 and ν_2 with corresponding fluxes F_{ν_1} and F_{ν_2}, α is given by

$$\alpha = \frac{\ln F_{\nu_1} - \ln F_{\nu_2}}{\ln \nu_1 - \ln \nu_2}. \tag{17}$$

In general, the intensity emitted at frequency ν by a column of material at temperature T is given by

$$I_\nu = B_\nu(T)(1 - e^{-\tau_\nu}), \tag{18}$$

where $B_\nu(T)$ is the Planck function, and τ_ν the optical depth at frequency ν. The spectral index α is then given by

$$\alpha \equiv \frac{d \ln I_\nu}{d \ln \nu} = \frac{d \ln B_\nu}{d \ln \nu} + \frac{\tau_\nu e^{-\tau_\nu}}{1 - e^{-\tau_\nu}} \left(\frac{d \ln \tau_\nu}{d \ln \nu} \right)$$
$$= \alpha_{Pl} + \frac{\beta \tau_\nu}{e^{\tau_\nu} - 1}, \tag{19}$$

where α_{Pl} is the spectral index of the Planck function and β is the logarithmic slope of the dust opacity. For optically thin emission, Equation (19) reduces to the relation $\alpha = \alpha_{Pl} + \beta$.

The observations of the spectral index presented in Galametz et al. (2019) are interpreted assuming a particular model for the temperature as a function of radius, which gives α_{Pl}. For the parameters of the sources considered in that paper, these model temperatures range from 20 to 43 K at a radius of 500 au. This assumption about the temperature allows them to estimate β.

We define $\beta_{1,3}$ to be the slope of the dust opacity between the frequencies corresponding to 1.3 mm and 3.2 mm. This quantity, reported in Galametz et al. (2019), depends both on the dielectric function of the dust as well as on the size distribution. For silicate dust, $\beta_{1,3}$ is about 1.6 for a size distribution composed of grains much less than 1 mm in size, and becomes 0 for grains much larger than 3 mm in size.

$\beta_{1,3}$ is about 1.5 in the diffuse ISM (Planck Collaboration et al. 2014). The values in Galametz et al. (2019) at 500 au range from 0.44 to 1.41, with a mean of 0.82, and are even lower at smaller distances from the star. We can estimate how cold the emitting dust must be for these values of $\beta_{1,3}$ to arise from an incorrect assumption about the temperature. For a typical temperature of 30 K at 500 au, $\alpha_{\rm Pl}^{1,3} = 1.87$, where $\alpha_{\rm Pl}^{1,3}$, analogous to $\beta_{1,3}$, is the slope of the Planck function between the frequencies corresponding to 1.2 and 3.3 mm. If in reality the temperature were lower, then $\alpha_{\rm Pl}^{1,3}$ would be lower too, and the method of Galametz et al. (2019) would underestimate $\beta_{1,3}$. However, to underestimate $\beta_{1,3}$ by 0.7 due to temperature effects, the true value of $\alpha_{\rm Pl}^{1,3}$ would have to be 1.17. This would require a temperature of 6 K, an implausibly low number in protostellar environments. The difference between 20 K and 43 K (the highest and lowest temperatures used in the modeling in Galametz et al. 2019 at 500 au) corresponds to a difference in $\alpha_{\rm Pl}$ of only 0.1. For this reason, we do not consider low temperature to be a plausible explanation for the low spectral indices.

As can be seen from Equation (19), a finite value of the optical depth will lower the observed α. However, it was shown in Galametz et al. (2019) that the optical depths at 1.3 mm were only of order 0.1 at 500 au. This was deduced from $\tau_\nu = -\ln(1 - I_\nu/B_\nu)$, by comparing the intensity I_ν of the observed emission with the intensity of a blackbody at the assumed temperature. Again, if the true temperature were smaller by a factor of a few than the temperature they assumed, then their results would imply an optical depth of order unity, but this seems implausible. Assuming $\beta = 1.5$, it would require an optical depth at 1.3 mm of 0.25 to reduce the inferred β by 0.1, and of 2.2 to reduce the inferred β by 0.7 (i.e., from 1.5 down to the 0.8—the mean of the observations at 500 au).

3.2.2. Scattering

In recent years, it has been realized that, as grains grow, the scattering cross section at millimeter wavelengths becomes important and cannot be neglected in high optical depth regions (e.g., see the discussion in Miotello et al. 2022). The effect of scattering may also modify the emission in high optical depth regions to appear as regions with moderate optical depth when interpreted in a classical fashion (see, e.g., Zhu et al. 2019). It is important to realize that, for scattering to be relevant, grains need to have grown to a significant fraction of the observing wavelength. This effectively implies that, even considering the effects of scattering, when $T_d \gtrsim 20$ K, a low measured value of $\beta_{1,3}$ associated with a moderate optical depth necessarily implies the presence of grain growth to sizes exceeding 100 μm.

3.2.3. Spinning Dust Emission

An additional possible explanation for the anomalous spectral index is contamination of the emission by something other than thermal emission. In some of the studies motivating this work, it has been shown that the spectral indices between 1.3 and 3.2 mm can be contaminated by synchrotron radiation (Galametz et al. 2019), and free–free emission (Miotello et al. 2014; Galametz et al. 2019). In this section, we consider also the possibility that electric dipole emission from spinning dust (Draine & Lazarian 1998) could be a contaminant.

To evaluate this, we used the SpDust code[6] (Ali-Haïmoud et al. 2009; Silsbee et al. 2011). We calculated the spinning dust emissivity at a hydrogen number density of $10^7 \, {\rm cm}^{-3}$ and at temperatures of 20 and 40 K. We assumed the fiducial strength of the grain dipole moment from Silsbee et al. (2011). The grain size distribution was assumed to be that given in line 16 of Table 1 of Weingartner & Draine (2001). This corresponds to somewhat evolved dust with $R_V = 5.5$, but it still contains a negligible number of grains with sizes greater than 2 microns. We stress that the spinning dust emission is dependent on the presence of nm-sized particles, whose abundance in such regions is very uncertain. While simple modeling suggests that such small grains would have been removed from the size distribution very efficiently via coagulation (Silsbee et al. 2020), PAHs have been detected in protoplanetary disks (Seok & Li 2017). Indeed, modeling in such disks (Hoang et al. 2018) shows that spinning dust emission can dominate over thermal emission at wavelengths $\gtrsim 3$ mm. Assuming this grain size distribution, in Figure 2 we plotted the emissivity per hydrogen atom from thermal dust emission (dashed lines), spinning dust emission (dotted lines), and their combination (solid lines). Red curves correspond to an assumed gas temperature of 40 K and blue to a gas temperature of 20 K. The thermal dust emission was calculated using Mie theory, assuming the dust and gas temperatures to be equal. The dielectric functions for silicate and carbonaceous grains are given in Draine (2003). We see that the spinning dust emission is completely irrelevant at 1.3 mm, but may substantially influence the observations at 3.2 mm. The role of such emission could be clarified with more wavelength coverage, i.e., if observations were made with ALMA band 4 (as the longest wavelength where we expect no contribution from spinning dust) as well as in bands 1 and 2 (which would directly constrain the spinning dust contribution).

For ν_1 and ν_2, corresponding to emission at 1.3 and 3.2 mm, the spectral indices are $\alpha = 3.48$ and $\alpha = 3.58$ for $T = 20$ K and $T = 40$ K, respectively. However, when we include also the spinning dust emission, these values drop to 3.22 and 2.28, respectively. A value of $\alpha = 2.28$, interpreted as arising from thermal dust emission at 40 K, would imply $\beta_{1,3} = 0.4$, equal to the lowest of the measurements in Galametz et al. (2019). That said, counter to the expectation if spinning dust emission were important, we note that there is essentially no correlation between the estimated temperature and the spectral index in the sources shown in Table 2 of Galametz et al. (2019). In summary, we consider spinning dust to be an interesting possibility that cannot as of now be ruled out.

4. Conclusion

Several recent observations of dust emission in the envelopes of young protostars have shown that the emission in the wavelength range between 1 and 3 mm has a spectral index much below what would be expected if the emission were dominated by thermal emission from small ($\ll 1$ mm)

---

6 https://cosmo.nyu.edu/yacine/spdust/spdust.html
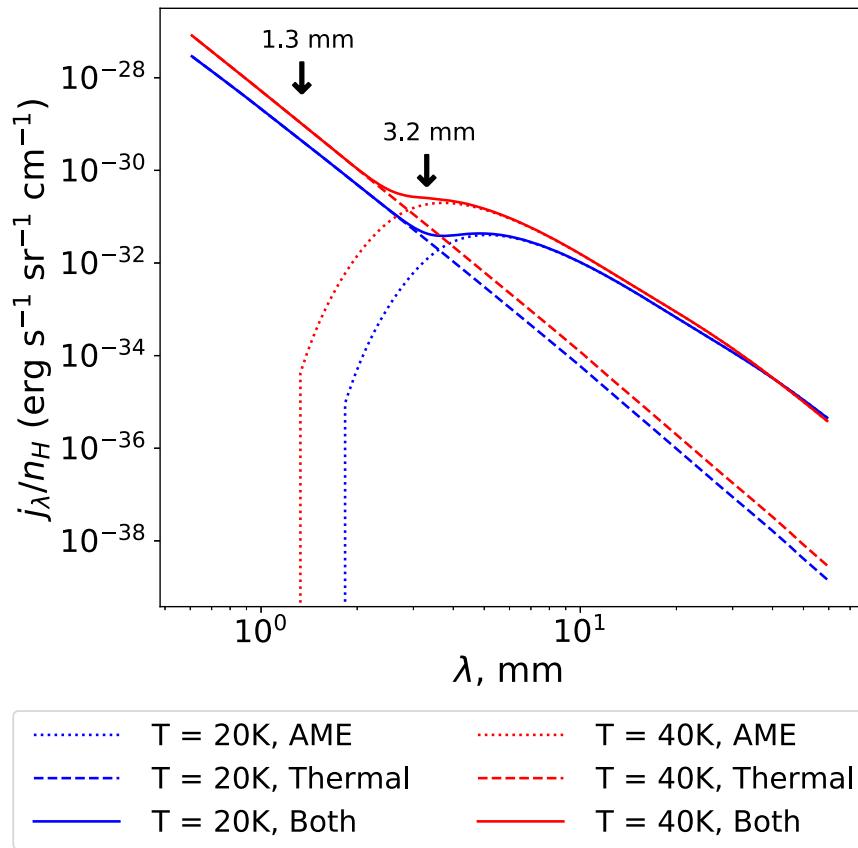
Figure 2. Emissivity per hydrogen atom from thermal emission (dashed lines), spinning dust emission (dotted lines), and the combination (solid lines). Blue curves correspond to an assumed gas temperature of 20 K, and red curves to an assumed gas temperature of 40 K. The arrows show the locations of the two wavelengths observed in Galametz et al. (2019).

dust grains. This has been put forth as evidence for grain growth to millimeter sizes, but this interpretation is in tension with coagulation simulations that do not allow the coagulation of such grains in the relevant timescales. Due to the large number of parameters controlling grain growth, it is difficult to make a definitive statement based on a tractable number of numerical simulations. For that reason, we developed an analytic model of the grain growth and tested it against simulations.

The key result of this paper is given by Equation (16), which shows the maximum "optical equivalent" size a_{opt} to which a grain can grow (for porous grains, this is the size of a compact grain with similar optical properties). This exact formula shows that a_{opt} only depends on the product of gas density n_g, the threshold velocity v_{max} for grain fragmentation, and the lifetime τ_{env} of the gaseous envelope. For a threshold velocity of $10 \, \mathrm{m \, s^{-1}}$, typical lifetimes of Class 0 protostars (10^5 yr), and envelope densities $\leqslant 10^7 \, \mathrm{cm^{-3}}$, this shows that grain growth cannot proceed to an equivalent size more than a few microns. In order for mm-sized grains to form, this product would have to increase by two orders of magnitude, which we consider implausible.

We consider other possible explanations for the low spectral index. These include the effects of optical depth and temperature (which seem unlikely to contribute significantly) as well as possible (but poorly constrained) features in the dielectric function of the ices on the dust. We also considered the possibility that the emission at long wavelengths is contaminated by electric dipole emission from the smallest dust grains. This is plausible, but would require the presence of a large population of ∼nm sized grains. It is also possible that large grains are present in the envelopes, but are not grown in situ. An attractive option could be rapid growth in disks followed by extraction and redistribution in the envelope via powerful protostellar outflows (Wong et al. 2016; Tsukamoto et al. 2021).

Appendix
## Verification of Assumptions

We verified with coagulation simulations that Equation (9) provides a good approximation of the evolution of the dust size. The left panel in Figure 3 shows a comparison between a more accurate calculation of the collision velocities between grains of equal sizes made in Gong et al. (2021) and the analytic approximation made in Equation (6). The curves from Gong et al. (2021) take into account both a dissipation scale for the turbulence as well as Brownian motion. These curves are essentially identical to those used in this paper for grains larger than 10 microns.

The right panel of the plot shows a comparison between the average grain size found in the simulation and that predicted by Equation (9). The simulations were started with all grains having a size of $a_0 = 1\,\mu$m, and assuming that grains remain compact with $D = 3$.

The curves are different for two reasons. First, the collision velocities used in the simulation are initially substantially smaller because of the assumed turbulence dissipation at small scales. This effect becomes unimportant once growth has proceeded well past the size at which the collision velocities in Equation (6) match those used in the simulation. Second, our assumption of a monodisperse size distribution is not exactly correct, which could in principle affect the results at all sizes. However, we see that in all cases the curves converge to much better than a factor of 2 at large sizes, where the collision velocities are the same.

We note that, although the minimum eddy size is uncertain, this uncertainty can only serve to hinder the formation of large grains. If the minimum eddy size were larger than that used in the calculation of the left panel of Figure 3, then the cutoff (seen below 10^{-3} cm) would occur for larger sizes and the coagulation would be further delayed. This cutoff, provided it is not above the maximum grain size, will not affect the relationship between v_g and v_{max}. Therefore, its presence can only act to slow down grain coagulation.
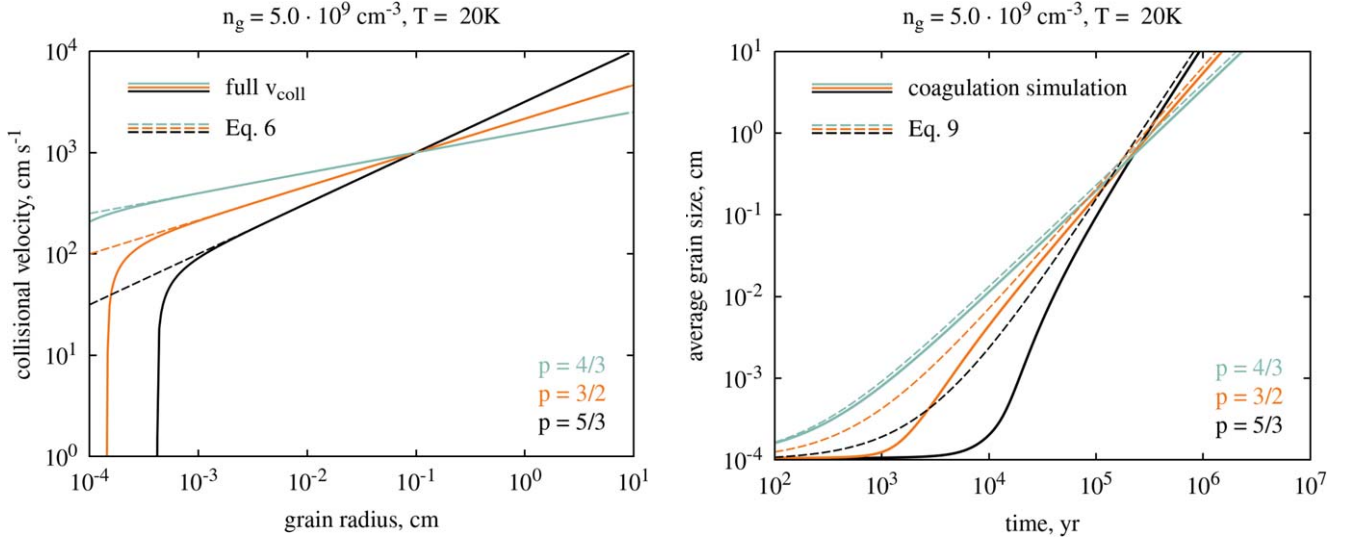
Figure 3. Collisional velocities between grains of equal size (left) and average grain size evolution (right) for the numerical and analytical coagulation models (solid and dashed lines). The turbulent Mach number $M = v_g/c_s$ is set to 0.24, 0.51, and 1.17 for MRI ($p = 4/3$), Iroshnikov–Kraichnan ($p = 3/2$), and Kolmogorov ($p = 5/3$) turbulence, respectively, resulting in collision velocities of 10 m s^{-1} for 1 mm grains.

ORCID iDs

Kedron Silsbee ⓘ https://orcid.org/0000-0003-1572-0505
Vitaly Akimkin ⓘ https://orcid.org/0000-0002-4324-3809
Alexei V. Ivlev ⓘ https://orcid.org/0000-0002-1590-1018
Leonardo Testi ⓘ https://orcid.org/0000-0003-1859-3070
Munan Gong ⓘ https://orcid.org/0000-0003-1613-6263
Paola Caselli ⓘ https://orcid.org/0000-0003-1481-7911

References

Agurto-Gangas, C., Pineda, J. E., Szűcs, L., et al. 2019, A&A, 623, A147
Akimkin, V. V., Ivlev, A. V., & Caselli, P. 2020, ApJ, 889, 64
Ali-Haïmoud, Y., Hirata, C. M., & Dickinson, C. 2009, MNRAS, 395, 1055
Allodi, M. A., Ioppolo, S., Kelley, M. J., McGuire, B. A., & Blake, G. A. 2014, PCCP, 16, 3442
Asplund, M., Grevesse, N., Sauval, A. J., & Scott, P. 2009, ARA&A, 47, 481
Bate, M. R. 2022, MNRAS, 514, 2145
Birnstiel, T., Klahr, H., & Ercolano, B. 2012, A&A, 539, A148
Blum, J., & Wurm, G. 2008, ARA&A, 46, 21
Draine, B. T. 2003, ApJ, 598, 1026
Draine, B. T., & Lazarian, A. 1998, ApJ, 508, 157
Epstein, P. S. 1924, PhRv, 23, 710
Evans, N. J. I., Dunham, M. M., Jørgensen, J. K., et al. 2009, ApJS, 181, 321
Galametz, M., Maury, A. J., Valdivia, V., et al. 2019, A&A, 632, A5
Giuliano, B., Gavdush, A., Müller, B., et al. 2019, A&A, 629, A112
Gong, M., Ivlev, A. V., Akimkin, V., & Caselli, P. 2021, ApJ, 917, 82
Gong, M., Ivlev, A. V., Zhao, B., & Caselli, P. 2020, ApJ, 891, 172
Guillet, V., Hennebelle, P., Pineau des Forêts, G., et al. 2020, A&A, 643, A17
Gundlach, B., & Blum, J. 2015, ApJ, 798, 34
Hirashita, H., & Omukai, K. 2009, MNRAS, 399, 1795
Hoang, T., Lan, N.-Q., Vinh, N.-A., & Kim, Y.-J. 2018, ApJ, 862, 116
Kataoka, A., Okuzumi, S., Tanaka, H., & Nomura, H. 2014, A&A, 568, A42
Kimura, H., Wada, K., Senshu, H., & Kobayashi, H. 2015, ApJ, 812, 67
Kimura, H., Wada, K., Kobayashi, H., et al. 2020, MNRAS, 498, 1801
Könyves, V., André, P., Men'shchikov, A., et al. 2015, A&A, 584, A91
Kristensen, L. E., van Dishoeck, E. F., Bergin, E. A., et al. 2012, A&A, 542, A8
Kwon, W., Looney, L. W., Mundy, L. G., Chiang, H.-F., & Kemball, A. J. 2009, ApJ, 696, 841
Li, J. I. H., Liu, H. B., Hasegawa, Y., & Hirano, N. 2017, ApJ, 840, 72
Miotello, A., Kamp, I., Birnstiel, T., Cleeves, L. I., & Kataoka, A. 2022, arXiv:2203.09818
Miotello, A., Testi, L., Lodato, G., et al. 2014, A&A, 567, A32
Musiolik, G., Teiser, J., Jankowski, T., & Wurm, G. 2016, ApJ, 818, 16
Okuzumi, S., Tanaka, H., & Sakagami, M.-a. 2009, ApJ, 707, 1247
Ormel, C. W., Paszun, D., Dominik, C., & Tielens, A. G. G. M. 2009, A&A, 502, 845
Ossenkopf, V. 1993, A&A, 280, 617
Ossenkopf, V., & Henning, T. 1994, A&A, 291, 943
Pagani, L., Steinacker, J., Bacmann, A., Stutz, A., & Henning, T. 2010, Sci, 329, 1622
Planck Collaboration, Abergel, A., Ade, P. A. R., et al. 2014, A&A, 566, A55
Rossi, S. C. F., Benevides-Soares, P., & Barbuy, B. 1991, A&A, 251, 587
Seok, J. Y., & Li, A. 2017, ApJ, 835, 291
Shen, Y., Draine, B. T., & Johnson, E. T. 2008, ApJ, 689, 260
Silsbee, K., Ali-Haïmoud, Y., & Hirata, C. M. 2011, MNRAS, 411, 2750
Silsbee, K., Ivlev, A. V., Sipilä, O., Caselli, P., & Zhao, B. 2020, A&A, 641, A39
Testi, L., Birnstiel, T., Ricci, L., et al. 2014, in Protostars and Planets VI, ed. H. Beuther et al. (Tucson, AZ: Univ. Arizona Press), 339
Tsukamoto, Y., Machida, M. N., & Inutsuka, S.-i. 2021, ApJL, 920, L35
Valdivia, V., Maury, A., Brauer, R., et al. 2019, MNRAS, 488, 4897
Wada, K., Tanaka, H., Okuzumi, S., et al. 2013, A&A, 559, A62
Wada, K., Tanaka, H., Suyama, T., Kimura, H., & Yamamoto, T. 2008, ApJ, 677, 1296
Weingartner, J. C., & Draine, B. T. 2001, ApJ, 548, 296
Wong, Y. H. V., Hirashita, H., & Li, Z.-Y. 2016, PASJ, 68, 67
Zhu, Z., Zhang, S., Jiang, Y.-F., et al. 2019, ApJL, 877, L18